

A global flood risk modeling framework built with climate models and machine learning

David A. Carozza¹, Mathieu Boudreault¹

¹Département de mathématiques, Université du Québec à Montréal, Montréal, QC, Canada

Key Points:

- We present a global flood model built using machine learning methods fitted with historical flood occurrences and impacts
- Forced with a climate model, the global flood model is fast, flexible and consistent with global climate
- We provide global flood hazard (occurrence) and risk (population displaced) maps over 4734 watersheds

Corresponding author: David A. Carozza, david.carozza@gmail.com

Abstract

Large scale flood risk analyses are fundamental to many applications requiring national or international overviews of flood risk. While large-scale climate patterns such as teleconnections and climate change become important at this scale, it remains a challenge to represent the local hydrological cycle over various watersheds in a manner that is physically consistent with climate. As a result, global models tend to suffer from a lack of available scenarios and flexibility that are key for planners, relief organizations, regulators, and the financial services industry to analyze the socioeconomic, demographic, and climatic factors affecting exposure. Here we introduce a data-driven, global, fast, flexible, and climate-consistent flood risk modeling framework for applications that do not necessarily require high-resolution flood mapping. We first use statistical and machine learning methods to examine the relationship between historical (from the Dartmouth Flood Observatory) flood occurrence and impact, and climatic, watershed, and socioeconomic factors at over 4700 watersheds globally. Using bias-corrected output from the NCAR CESM Large Ensemble from 1980 to 2020, and the fitted statistical relationships, we simulate one million years of events worldwide along with the population displaced. We discuss potential applications of the model and present global flood hazard and risk maps. The main value of this global flood model lies in its ability to quickly simulate realistic flood events at a resolution that is useful for large-scale socioeconomic and financial planning, yet we expect it to be useful to climate and natural hazard scientists who are interested in socioeconomic impacts of climate.

Plain Language Summary

Flood is among the deadliest and most damaging natural disasters. To protect against flood risk at large scales, stakeholders need to understand how floods can occur and their potential impacts. Stakeholders rely heavily on global flood models to provide them with plausible flood scenarios around the world. For a flood model to operate at the global scale, climate effects must be represented in addition to hydrological ones to demonstrate how rivers can overflow throughout the world each year. Global flood models often lack the flexibility and variety of scenarios required by many stakeholders because they are computationally demanding. Designed for applications where detailed local flood impacts are not required, we introduce a rapid and flexible global flood model that can generate hundreds of thousands of scenarios everywhere in the world in a matter of minutes. The model is based on a historical flood database that is represented using an algorithm that learns from the data. With this model, the output from a global climate model is used to simulate a large sample of floods for risk analyses that are coherent with global climate. Maps of the annual average number of floods and number of displaced people illustrate the models results.

1 Introduction

Flood is consistently among the most damaging natural disasters in terms of economic losses (Gall et al., 2009) and mortality (Hu et al., 2018). Impacts generated by flood result from a complex set of interactions between climatic, hydrological, demographic, and economic factors. Despite improvements in flood defenses and other technologies resulting in reduced vulnerability (Paprotny et al., 2018), nominal flood-related economic losses have increased rapidly in recent decades due to developments in exposure such as total wealth and urban area (Jongman et al., 2012), and rising prices. After normalizing relative to exposure, Barredo (2009) and Neumayer and Barthel (2011) did not identify statistically significant increasing trends in economic flood losses, yet short time series, challenges with data, and the inability to control for changes in flood defenses challenged these studies. Trends in insured losses, which are further complicated by the extent to which exposure is insured, were not found for atmospheric natural disasters at

62 the global scale (Barthel & Neumayer, 2011). However, the same study detected a posi-
63 tive trend in normalized flood-driven insured losses from 1980-2007 in the United States.
64 Paprotny et al. (2018) reconstructed floods in Europe since 1870 and uncovered increas-
65 ing trends in normalized flooded area and persons affected but decreases in normalized
66 fatalities and financial losses in recent decades.

67 Large scale flood risk analyses are pivotal to disaster management and relief plan-
68 ning at regional, national, and international levels. Flood risk analyses can build resilience
69 by informing investment needs in mitigation and financial mechanisms such as insurance
70 (Vorogushyn et al., 2018). By the nature of their business, insurance and reinsurance com-
71 panies are heavily exposed to flood risk across the globe through private and/or pub-
72 lic insurance programs (OECD, 2016), whereas banks are subject to mortgage defaults
73 following floods (FRBSF, 2019; Ouazad & Kahn, 2019). With mounting pressure com-
74 ing from regulators and other bodies worldwide, the financial services industry (banks,
75 insurers and reinsurers) will soon need to disclose and stress test their solvency and sta-
76 bility to various climate scenarios (Bank of England, 2019; Task Force on Climate-related
77 Financial Disclosures, 2017), which includes how future flood risk will affect their prof-
78 itability.

79 A major methodological challenge to designing global models is to guarantee that
80 flood risk is consistent from climate, hydrological, hydraulic, and exposure standpoints,
81 such that physically-consistent global climate patterns drive the local hydrological cy-
82 cle over many watersheds (Vorogushyn et al., 2018). This is a particularly important is-
83 sue for the financial services industry as their global portfolios are impacted by large-
84 scale climate patterns affecting people over distances of thousands of kilometers. Top
85 down approaches typically force low-resolution hydrological models with meteorologi-
86 cal or climate model outputs that simulate runoff that is consistent with simulated cli-
87 mate patterns (Yamazaki et al., 2011; Winsemius et al., 2013). Such approaches are not
88 just global because they represent the entire planet, but because connections between
89 basins in space that are driven by climate are resolved. Top down methods have been
90 used to delve into large-scale flood risk questions such as examining patterns of inter-
91 annual climate variability (Ward et al., 2014) and to project the impacts of future cli-
92 mate and socioeconomic change (Jongman et al., 2014; Dottori et al., 2018; Ward et al.,
93 2020). An important weakness of this approach is its lack of focus on flooding occurrence
94 and impact in itself, and the inability to resolve small scale floods.

95 Bottom up approaches consider higher resolution processes that employ a combi-
96 nation of rainfall-runoff or hydrological modeling to drive a hydraulic component and
97 calculate flood damage over watersheds (de Bruijn et al., 2014; Sampson et al., 2015; Fal-
98 ter et al., 2016). These models are typically forced by meteorological (historical, simu-
99 lated, or projected) or discharge distributions. This more detailed approach is closer to
100 assessing localized impacts of flood but is challenged by high computational demands
101 and data requirements that are not necessarily available globally (Ward et al., 2015). For
102 both approaches, the number of scenarios available is limited and they lack the flexibil-
103 ity required by planners, relief organizations, regulators, and the financial services in-
104 dustry to analyze the socioeconomic, demographic, and climatic factors affecting expo-
105 sure.

106 In this paper, we introduce a data-driven, global, fast, flexible and climate-consistent
107 flood risk modeling framework for applications that do not necessarily require high-resolution
108 flood mapping. Our framework is unique in that it is driven by historical flood and en-
109 vironmental observations. It takes advantage of the speed of statistical models to quickly
110 generate large global catalogues of flood events that are physically consistent with cli-
111 mate. Distributions of occurrence and impact can then be analyzed in terms of climatic
112 and socioeconomic factors and over spatial scales of interest. The framework is there-
113 fore capable of examining interannual climate variability and looking into the future, ac-
114 counting for global change over various greenhouse gas emission and socioeconomic sce-

115 narios, in addition to accounting for climate-driven connections between basins. Appli-
 116 cations of the model include socioeconomic studies, climatic research of the impacts on
 117 population or wealth affected, risk analyses in poorly sampled watersheds (Hrachowitz
 118 et al., 2013), and stress testing risk portfolios for the financial services industry.

119 To expand upon the limited observational record (Munoz & Dee, 2017), we gener-
 120 ate a large sample of flood occurrence probabilities and impacts using bias-corrected
 121 precipitation and temperature output from the National Center for Atmospheric Research’s
 122 (NCAR) Community Earth System Model (CESM) Large Ensemble (LE) (Kay et al.,
 123 2015) for each watershed, ensemble member, and model hydrological year for the time
 124 period 1980-2020. The occurrence and impact components are fitted with large databases
 125 of past flood history that associate observed flood events to historical precipitation, tem-
 126 perature and watershed information such as topography, land use, soil type, and bedrock
 127 features using a machine learning method. Using the fitted occurrence and impact mod-
 128 els, we use stochastic simulation to generate a large global catalog of synthetic flood events
 129 along with impacts, expressed in terms of the population displaced and the gross domes-
 130 tic product affected in a watershed.

131 Section 2 presents the datasets used and Section 3 the model development. We eval-
 132 uate the quality and realism of the flood model in Section 4, present results that illus-
 133 trate the model’s capabilities in Section 5, and conclude in Section 6. A Supporting In-
 134 formation document is available online that presents supplementary description and val-
 135 idations.

136 2 Data

137 We base statistical models of flood occurrence and impact on two databases de-
 138 tailed here that associate flood events and their consequences to the driving environmen-
 139 tal and demographic conditions. The global flood model is represented in terms of wa-
 140 tersheds from HydroBASINS (Lehner & Grill, 2013). Observations of flood occurrence
 141 and impact, in terms of population displaced, are derived from the Dartmouth Flood Ob-
 142 servatory Global Active Archive of Large Flood Events (Brakenridge, 2010). Environ-
 143 mental quantities that drive flood are represented in terms of a variety of sources that
 144 include climatological quantities such as precipitation (Xie et al., 2007; Funk et al., 2015)
 145 and temperature (Shi, 2007), and watershed characteristics such as: topography and lo-
 146 cation (Lehner & Grill, 2013; Marthews et al., 2015b), land cover and vegetation state
 147 (Latham et al., 2014), soil type (Shangguan et al., 2014), depth to bedrock (Shangguan
 148 et al., 2017), and hydrogeologic properties (Gleeson et al., 2014). Population (Doxsey-
 149 Whitfield et al., 2015; Klein Goldewijk et al., 2017) and wealth (Kummu et al., 2018)
 150 are used as demographic characteristics (Table 1).

151 To generate the global flood catalogue of events, we force the flood occurrence and
 152 impact models with output from the CESM Large Ensemble (CESM-LE) Community
 153 Project (Kay et al., 2015) that is driven by the NCAR Community Earth System Model
 154 (CESM1) (Hurrell et al., 2013). We apply precipitation quantities from the Community
 155 Land Model 2.0 (Lawrence et al., 2011) and temperature from the Community Atmo-
 156 sphere Model 5.2 (Neale et al., 2012) (Table 2).

157 3 Model

158 A riverine flood and its impact is driven by 1. an excess of precipitation less evap-
 159 otranspiration relative to the storage capacity of the watershed, and 2. interaction with
 160 the population affected. We built a statistical framework for flood risk that relates flood
 161 occurrence and impact to environmental and demographic predictor variables (Table 1)
 162 at the watershed scale. Wolock et al. (2004) and Rumsey et al. (2015) used a similar sta-
 163 tistical framework to define hydrologic-landscape regions and estimate baseflow, respec-

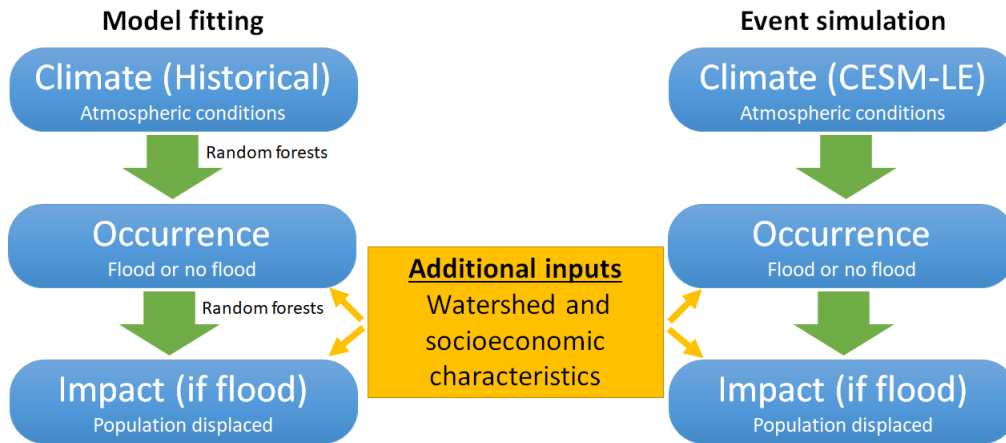


Figure 1. Schematic of the model components. The fitting process is detailed on the left, whereas the simulation process is presented on the right.

164 tively, but to the authors’ knowledge such an approach has not been applied to flood risk
 165 modeling at the global scale. While our approach falls into the class of lumped models
 166 (Bevin, 2012; Perrin et al., 2013) since the forcing data we used is averaged over a wa-
 167 tershed, instead of considering a system output quantity such as discharge, we directly
 168 model watershed 1. flood hazard and 2. impact. We achieve this by building databases
 169 and statistical models of 1. flood occurrence and 2. the fraction of population displaced,
 170 and express them in terms of environmental and demographic predictor variables. The
 171 model components are summarized in Figure 1.

172 3.1 Data Inputs

173 3.1.1 Observational Data

174 Historical flood events are provided by the Dartmouth Flood Observatory (DFO)
 175 Global Active Archive of Large Flood Events (Brakenridge, 2010). DFO flood events are
 176 derived from news, government, and instrumental sources, and validated by satellite ob-
 177 servations. Floods are represented in space by means of a polygon that bounds the flooded
 178 areas (Figure 2). While this inherently overestimates flooded areas, it represents the syn-
 179 optoc and climatic scales over which riverine flood is driven and so is an appropriate quan-
 180 tity to quantify the association between climate variables and observed large-scale floods.
 181 All events with a non-atmospheric cause (Jökulhaup, tsunami, tides, avalanche, storm
 182 surge, barrier break or release, ice jam or ice break-up or ice melt) were ignored. We con-
 183 sidered the years 1985-2017, during which there were 4499 flood events globally.

184 Flood hazard and risk are represented at the level of watersheds whose boundaries
 185 are defined by the HydroBASINS (Lehner & Grill, 2013) dataset at Pfafstetter level 5,
 186 which unless otherwise stated we refer to simply as watersheds. The databases built here
 187 and all analyses are conducted over the 4734 watersheds at this scale (Figure 3). The
 188 historical flood occurrence and impact databases described are based on the spatial in-
 189 tersection of the DFO events and the HydroBASINS watersheds, which we refer to as
 190 watershed-floods. A single observed DFO flood event generally occurs over several wa-
 191 tersheds and therefore results in one or more watershed-floods. Due to the bounding poly-
 192 gon nature of the DFO flood events, we assumed that watershed-floods that are less than
 193 5% of the watershed area are “no flood” in our database. Based on an investigation into
 194 a subset of DFO events with 0 reported people displaced, we treated such floods as miss-

Observed DFO Flood Events

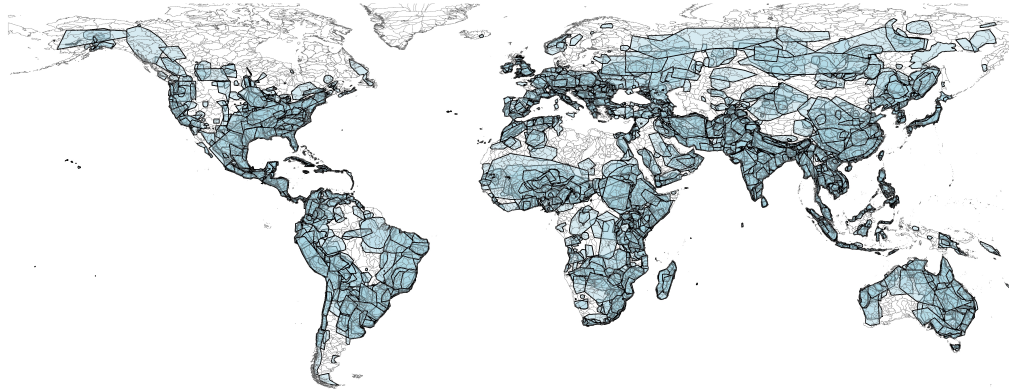


Figure 2. Dartmouth Flood Observatory flood events from 1985-2017.

HydroBASINS Level 5 Watersheds

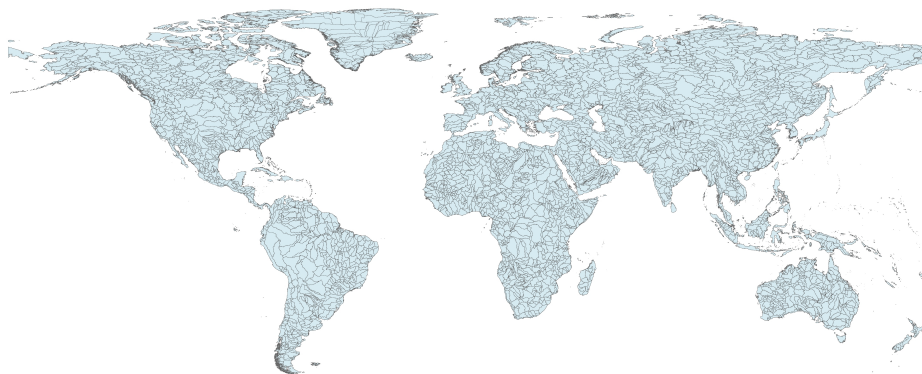


Figure 3. Graphical representation of the 4734 HydroBASINS level 5 watersheds.

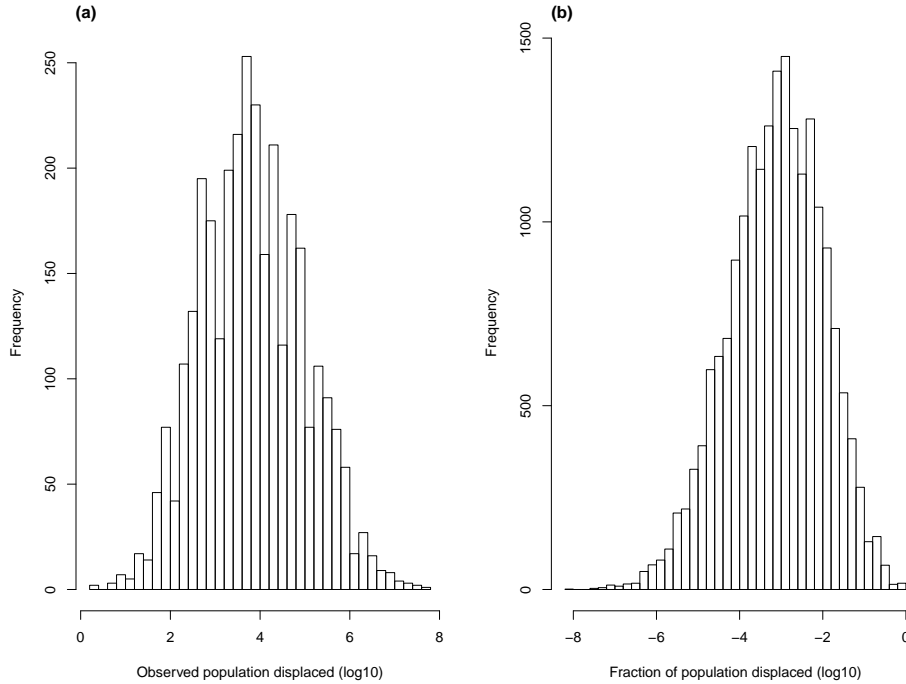


Figure 4. Distributions of population displaced impact variable. (a) Observed population displaced (\log_{10}) for each DFO event. (b) Fraction of population displaced (\log_{10}) for each watershed-event.

195 ing data instead of events with zero impact. These steps resulted in 3160 of the 4499 DFO
 196 floods with at least 1 person displaced (Figure 4a). For each flood, we distributed the
 197 population displaced over the watershed-floods in proportion to the population of the
 198 watershed in the year of the flood (Figure 4a).

199 We explored time-varying environmental predictors and chose datasets with the
 200 following features: 1. global spatial coverage, 2. temporal coverage that contained the
 201 DFO flood event dataset (1985-2017), 3. at least 1° spatial resolution, 4. at least daily
 202 temporal resolution, 5. resolved in the CESM-LE climate product that drives the cat-
 203 alogue simulation. While observational products such as soil moisture (Gruber et al., 2019)
 204 and terrestrial water storage (Tapley et al., 2004) were of interest, our restrictions lim-
 205 ited our analyses to precipitation and temperature products.

206 Precipitation is the key driving predictor to flood occurrence and impact. We rep-
 207 resent it using the Climate Hazards group Infrared Precipitation with Stations (CHIRPS)
 208 dataset (Funk et al., 2015) for latitudes from 50°S to 50°N , and the CPC Global Uni-
 209 fied Gauge-Based Analysis of Daily Precipitation (CPC Precipitation) dataset (Xie et
 210 al., 2007) for all other latitudes. Temperature plays a key role in evapotranspiration (Li
 211 et al., 2016) and we represent it with the CPC Global Daily Temperature (CPC Tem-
 212 perature) dataset (Shi, 2007). We considered several timescales of precipitation and tem-
 213 perature to capture potential regimes of climatic trajectories that can result in flood, namely
 214 averages over the 7, 8-30, 31-60, and 61-120 days prior to an event.

215 The remaining environmental predictors represent watershed storage capacity. Wate-
 216 rshed topography is a crucial characteristic in hydraulic modeling that determines flows
 217 along the surface and subsurface and influences infiltration into the subsurface (Farr et

218 al., 2007). We represent topographic features and watershed location with the HydroBASINS
 219 (Lehner & Grill, 2013) and High-resolution global topographic index values (TI) (Marthews
 220 et al., 2015b) datasets. Land cover characteristics alter infiltration into the subsurface
 221 and can additionally influence evapotranspiration (Nie et al., 2011). We represent land
 222 cover with the Global Land Cover SHARE (GLC-SHARE) (Latham et al., 2014) dataset.
 223 Soil permeability affects infiltration (Wolock et al., 2004) and subsurface drainage (Yu
 224 et al., 2000), whereas soil depth is indicative of soil water storage. We represent soil type
 225 with the Global Soil Database (GSD) (Shangguan et al., 2014) and depth with the Global
 226 Depth to Bedrock (GDB) (Shangguan et al., 2017) dataset. Bedrock porosity and per-
 227 meability proxy subsurface storage and drainage, respectively (Wolock et al., 2004). We
 228 represent these quantities using the GLoBal HYdrogeology MaPS 2.0 (GLHYMPS 2.0)
 229 (Gleeson et al., 2014) dataset.

230 The exposure predictors population density and GDP (Gross Domestic Product)
 231 per capita are interpreted as time-varying proxies of urbanization and flood control that
 232 can additionally capture features of land cover and socioeconomic change that are not
 233 represented in the time-invariant GLC-SHARE dataset, and as such affect both hazard
 234 and impact. Population is represented with the Gridded Population of the World (GPW)
 235 (Doxsey-Whitfield et al., 2015) and Anthropogenic land-use estimates for the Holocene
 236 (HYDE3.2) (Klein Goldewijk et al., 2017) datasets, and wealth with the Gridded global
 237 datasets for GDP and HDI (Human Development Index) over 1990-2015 (GDPHDI) (Kummu
 238 et al., 2018). Temporal extrapolations of these variables are described in the Support-
 239 ing Information.

240 **3.1.2 Climate Model Output**

241 The climate component used in our global model applies the NCAR-CESM1 (Hurrell
 242 et al., 2013) Large Ensemble (CESM-LE) (Kay et al., 2015). The CESM-LE was designed
 243 to examine interannual climate variability in the context of anthropogenic climate change,
 244 and consists of 40 ensemble members run from 1920 to 2100. Each member is initialized
 245 with a roundoff error perturbation to the atmosphere in model year 1850, so that by 1920
 246 the members are independent of one another yet driven by the same forcing. The NCAR-
 247 LE employs a single historical forcing scenario up to 2005 and the RCP8.5 from 2006 to
 248 2100. In this paper, to be consistent with the flood observational record from DFO, we
 249 consider the years 1980 to 2020. This results in 40 years from 40 members, which we re-
 250 fer to as 1600 member-years of global climate model output that drive the flood occur-
 251 rence and impact models to generate a stochastic catalog of floods. As with the predic-
 252 tor variables used in the statistical fit step, for each climate forcing variable (Table 2)
 253 we aggregate by taking the average of grid points in each level 5 watershed.

254 CESM-LE atmospheric rain and snow are summed to model precipitation. Snow
 255 is assumed to melt immediately to water when it touches the ground at a bulk weight
 256 density of 100 kg m^{-3} corresponding to that of fresh snow (Meløysund et al., 2007). Bi-
 257 ases in the CESM-LE precipitation are corrected relative to CHIRPS and CPC Precip-
 258 itation, and biases in temperature are corrected relative to CPC Temperature, both us-
 259 ing the methodology of Hempel et al. (2013). When considering the correction of the num-
 260 ber of dry months, we instead use the fraction of dry months since our simulated dataset
 261 (CESM-LE, with 40 years of data) has a different sample size to the observations (CHIRPS,
 262 with 37 years of data). This bias correction approach is widely used in the hydrologi-
 263 cal and flood impact literature and separately corrects monthly means and daily vari-
 264 ability about the means, thereby preserving long-term observed trends. We apply the
 265 correction to precipitation and temperature aggregated over each level 5 basin.

266

3.2 Occurrence Component

267

268

269

270

271

272

273

274

275

276

This component of the model represents the occurrence of a riverine flood (“flood” or “no flood”) in a level 5 watershed given a set of observed or simulated predictor environmental variables. Watershed hydrology and river hydraulics that result in floods are complex processes with inherent nonlinear features and interactions between forcing variables. To break down this problem, we first represent how climatological, hydrological and basin-scale factors determine riverine flood occurrence globally and regionally in the model fitting step. Once these relationships are established at the watershed level, we use output from the climate component in addition to the basin-scale predictors to simulate flood occurrences. Combining these two steps results in a global flood hazard model.

277

3.2.1 Model Fitting

278

279

280

281

282

283

284

285

Given the observed watershed-floods, we assumed that a level 5 watershed can be in one of two states (“flood” or “no flood”) in a given hydrological year dating from October 1 - September 30. The 32 hydrological years considered in the DFO database and 4734 watersheds resulted in a potential of 151488 occurrence observations. Taking missing data in the predictors into consideration left us with 128494 observations for the fitting process. For the occurrence problem climate predictors, we use the mean annual temperature and for precipitation take the annual maxima of each of the 4 timescales considered over the hydrological year.

286

287

288

289

290

291

292

293

294

295

The statistical problem at hand is therefore a classification problem with the binary response variable (“flood”, “no flood”). We considered classical and machine learning methods such as logistic regressions (LR), random forests (RF, Breiman (2001)) and artificial neural networks (NN, McCulloch and Pitts (1943)) to solve this problem. Hastie et al. (2009) discuss the three methods in chapters 4, 15, and 11, respectively. Since it is difficult to define explicit functional forms and interaction terms between the predictor variables a priori, in particular given the variety of flood regimes that exist globally, we adopted a machine learning approach that builds such relationship from observations. Validation of the occurrence models are presented in Section 4.1 for the chosen model, as well as in the Supporting Information for the other models.

296

297

298

299

300

We first fit each of the three models globally, thereby providing one set of parameter estimates per model. To guarantee that local dynamics were appropriately represented in the global fit, we also made fits of each model on aggregations of watersheds at Pfafstetter level 2 (HS2). Since there are 62 watersheds at HS2, 62 parameter sets were fitted.

301

302

303

304

305

306

307

308

309

310

311

For the global occurrence fit we took a random sample of 70% of the observations as the training set for all models and conducted out-of-sample validation on the remaining 30%, the test set. Although normalization of the variables is only required for the NN models, to compare the models we normalized all predictor variables to the range $[0, 1]$. For the RF model we considered 500 decision trees and 5 randomly selected predictors, from among the 38, to decide which predictor is selected for each split. Regional occurrence fits by HS2 watersheds are also based on normalized predictors and to compare with the global fit we used the same training and test set. Given the smaller samples involved in fitting the regional models, we only apply a fit if more than 3% of observations in the region are “flood”. The structure of the RF models follows the global model, with 500 decision trees and 5 predictors considered for each split.

312

3.2.2 Event Simulation

313

314

To simulate floods we apply the fitted occurrence model to compute predicted flood occurrence probabilities (1600 member-years \times 4734 watersheds) using the bias corrected

315 precipitation and temperature outputs from the CESM-LE and the basin-scale environ-
 316 mental and socioeconomic variables. Flood occurrence, for each member-year and each
 317 watershed, thus follows a Bernoulli distribution whose only parameter represents the prob-
 318 ability of a riverine flood. The flood occurrence probability is unique for every ensem-
 319 ble member year and watershed (40 members x 40 years x 4734 watersheds). To gener-
 320 erate a large sample of flood events at the global scale, we sample from each of these Bernoulli
 321 distributions 625 times, resulting in a million simulated years.

322 **3.3 Impact Component**

323 The impact component models the number of people affected by a given flood. It
 324 aims to approximate the combined effects of the exposure (population, wealth, etc.) and
 325 its vulnerability. Combining the occurrence and impact components thus yields the global
 326 flood *risk* model.

327 **3.3.1 Model Fitting**

328 Combining the DFO population displaced with the level 5 watershed population
 329 (Doxsey-Whitfield et al., 2015; Klein Goldewijk et al., 2017), we model the fraction of
 330 the population displaced (displaced population / watershed population) to proxy the im-
 331 pact. We applied a log10 transformation to the fraction displaced since it spans 8 orders
 332 of magnitude (Figure 4b). The predictor variables used are the same as for the occur-
 333 rence model, with the important difference that the four timescales for temperature and
 334 precipitation are calculated for the final day of the event as reported in DFO. Overall,
 335 the impact model aims to explain the log10 of the fraction of population displaced as
 336 a function of demographics, wealth, climatological, and watershed predictors. The cli-
 337 matological and watershed predictors aim to capture the effects of the intensity of a flood
 338 on the fraction of population displaced whereas population density and wealth per capita
 339 aim to capture the vulnerability of a population.

340 There are 19746 watershed-floods in the impact database with complete response
 341 and predictor information. As in the statistical modeling for occurrence, we considered
 342 classical and machine learning methods, namely linear regressions, random forests and
 343 neural networks (see above references for details). Validation of the impact models are
 344 presented in Section 4.2 for the chosen model, as well as in the Supporting Information
 345 for the others.

346 The global impact model fitting procedure follows the occurrence model and takes
 347 70% of the observations to form the training set. All validations are done by applying
 348 the fitted model to the remaining 30% of observations. As the impact model is a regres-
 349 sion problem, both predictors and the response variable were normalized to the range
 350 $[0, 1]$. For the random forest fits, since there are 41 predictors, we consider 6 randomly
 351 selected predictors at each tree split and repeat this for 500 regression trees. Regional
 352 impact observations were also normalized and used the same training observations as the
 353 global fit. A regional model was fitted when there were at least 30 watershed-flood im-
 354 pact observations in the HS2 watershed.

355 **3.3.2 Event Simulation**

356 For each simulated flood event, we in turn simulate impact in terms of the frac-
 357 tion of the watershed population displaced. The impact depends on the bias-corrected
 358 temperature and precipitation from the CESM-LE, watershed characteristics (which are
 359 assumed to not change in time), and the population density and wealth observed in the
 360 watershed for the year of the event. We assume the log10 of the fraction of population
 361 displaced is normally distributed (Figure 4b). The mean of the flood impact distribu-
 362 tion is taken from the maximum of daily impact predictions over the hydrological year.

363 The standard deviation parameter is determined by calculating the root mean squared
 364 prediction error in each of 9 groups determined by watershed population density. This
 365 grouping preserves the observed structure of increasing and then flat prediction errors
 366 for watershed-floods that depend on population density (Supporting Information).

367 In summary, to model impact in any watershed and year, we sample from a nor-
 368 mal distribution whose 1. mean parameter is the largest daily simulated impact of the
 369 fraction of population displaced, and 2. standard deviation parameter is the root mean
 370 squared prediction error from the fitted model for the population density group of the
 371 watershed. This process is repeated for each simulated flood over the million years of the
 372 catalogue.

373 3.4 Validations and Variable Importance

374 The flood occurrence model is a binary classification problem. A good classifica-
 375 tion model should predict an event when there is really an event (a true positive). How-
 376 ever, when occurrences are rare, it is easy to be accurate most of the time by simply pre-
 377 dicting the event always (or never) occurs. As such, one needs to evaluate models by bal-
 378 ancing true positives (TP) and true negatives (TN) with false positives (FP) and false
 379 negatives (FN) (Fawcett, 2006; Powers, 2011). Such analyses are commonly summarized
 380 using the receiver operating characteristic (ROC) curve, a plot of the true positive rate
 381 ($TP/(TP+FN)$) versus the false positive rate ($FP/(FP+TN)$), which are both determined
 382 as functions of the cutoff probability used to define a predicted “flood”. The area un-
 383 der the ROC curve (AUC) is a summary measure that ranges from 0 to 1 and indicates
 384 the likelihood that the classification model can differentiate between “flood” and “no flood.”
 385 Values above 0.5 indicate that the model in question has the ability to differentiate be-
 386 tween classes. We report the AUC aggregated over HS2 watersheds if there are at least
 387 10 observations and at least 5 floods in the test set (Section 4.1 and Figure 5). Other
 388 model evaluation metrics are discussed in the Supporting Information.

389 To assess the quality of the impact models for the linear model (LM), random for-
 390 est (RF), and neural network (NN), we consider two metrics using out-of-sample obser-
 391 vations : the root mean square error (RMSE, lower is better) and the R-squared (higher
 392 is better, with 1 being the maximum). The RMSE summarizes the model error whereas
 393 the R-squared measures the proportion of variance explained by a model (Hastie et al.,
 394 2009) (Section 4.2 and Figures 6 and 7).

395 For the random forest models, we consider two variable importance measures for
 396 each of the flood classification and regression problems using the R `randomForest` pack-
 397 age (Liaw & Wiener, 2002). The first measure considers how the accuracy changes in
 398 reaction to permuting the observations of each predictor in the out-of-bag (a test set)
 399 observations. For occurrence, accuracy is defined as the fraction of observations that are
 400 correctly classified $(TP+TN)/(TP+TN+FP+FN)$, whereas for impact the mean
 401 squared error is used. The second measure employs node purity, which rewards homo-
 402 geneity in predictions. For flood occurrence, the Gini impurity index is used, whereas
 403 for impact the residual sum of squares is used.

404 3.5 Code and Computations

405 Our work was coded using the R software environment (R Core Team, 2018). We
 406 used the package `data.table` (Dowle & Srinivasan, 2018) for data processing and merg-
 407 ing, and `velox` (Hunziker, 2017) to calculate aggregations of the predictor and climate
 408 variables over the HydroBASINS watersheds. The packages `sp` (E. J. Pebesma & Bivand,
 409 2005) and `sf` (E. Pebesma, 2018) were applied for spatial analyses such as spatial inter-
 410 sections. The linear model and logistic regressions fits were achieved with the `stats` pack-
 411 age core functions `lm()` and `glm()` (R Core Team, 2018), and we applied the `randomForest`

412 (Liaw & Wiener, 2002) and `RSNNS` (Bergmeir & Benítez, 2012) packages for the RF and
 413 NN models. `ROCR` (Sing et al., 2005) was used for the occurrence model validation cal-
 414 culations and `doSNOW` (Microsoft & Weston, 2017) was used to parallelize computations.
 415 We used `cartography` (Giraud & Lambert, 2016) for choropleth maps and `RColorBrewer`
 416 (Neuwirth, 2014) for the color schemes.

417 Table 3 details the steps involved in simulating the flood catalogue. The durations
 418 reported are for a single processor thread on an Intel Xeon E5-2650 v3 at 2.30 GHz. Step
 419 2 takes approximately 1 day to compute daily impact predictions over the model years
 420 1980-2020 of the CESM-LE. While this is the most computationally demanding step, it
 421 takes only 37 minutes per ensemble member and so the duration of the user’s calcula-
 422 tions depend on the number of ensemble members of interest. All other steps are rapid,
 423 with the simulation of 1 million years of flood occurrence requiring only 14 minutes (Step
 424 1) and the simulation of corrected impacts and merging with occurrence taking only 39
 425 minutes (Step 8). While we worked with a single thread, step 2 can be parallelized given
 426 sufficient system memory, easily reducing the calculation by a factor of 6 to 8.

427 Simple shocks to the occurrence or impact components through the predictor vari-
 428 ables, such as precipitation or temperature, can be conveniently considered to examine
 429 model sensitivity. In particular, for monotonic shocks to individual predictors, Step 2
 430 need not be repeated since the predictors that generate the annual maximum are already
 431 known. The occurrence and impact prediction functions of the model can also be used
 432 with alternative precipitation and temperature output (for example another climate model,
 433 reanalysis product, or temperature or precipitation product), or socioeconomic data prod-
 434 ucts. For such an application, the user should first compare the statistical properties of
 435 the new forcing quantities over the watersheds of interest with those used in the model
 436 fitting. Based on those analyses, the user should consider applying a bias-correction be-
 437 fore proceeding with the steps described in Table 3.

438 4 Results and Model Validation

439 This section presents validations for the occurrence and impact models that we de-
 440 scribe in terms of goodness of fit, parsimony, ease of use, and interpretation (Sections
 441 4.1 and 4.2). Results are presented on world maps over aggregated HydroBASINS wa-
 442 tersheds. We analyze the realism of the entire simulated flood catalogue in Section 4.3.
 443 Additional validations and other results can be found in the Supporting Information.

444 4.1 Occurrence

445 Overall, we find that logistic regressions do poorly for the global fit but their qual-
 446 ity significantly improves when fitted regionally (Table 4 and Supporting Information).
 447 RF and NN models are built to capture complex non-linear relationships and interac-
 448 tions between predictors and given the problem at hand it is not a surprise that such non-
 449 linearities and interactions appear. As such, RF and NN perform similarly globally and
 450 over regional aggregations of watersheds. That said, for fits over HS2 watersheds, all three
 451 methods perform similarly.

452 Neural networks do not significantly improve the quality of the fit when compared
 453 to random forests. With only 128494 observations, the dataset is likely not in the ap-
 454 propriate sample size regime to observe the benefits of NNs. Given the difficulty in in-
 455 terpreting NNs, we cannot recommend their use for this application. We generally find
 456 that the RF, fitted globally or regionally, is a solid approach in terms of in-sample and
 457 out-of-sample fit of global flood occurrences. Given that the RF is composed of individ-
 458 ual decision trees applied to random samples of the observations, it is also easier to in-
 459 terpret than the other models. If a user has a preference toward a more statistical ap-
 460 proach, we recommend the use of logistic regressions in combination with regional fits.

AUC RF

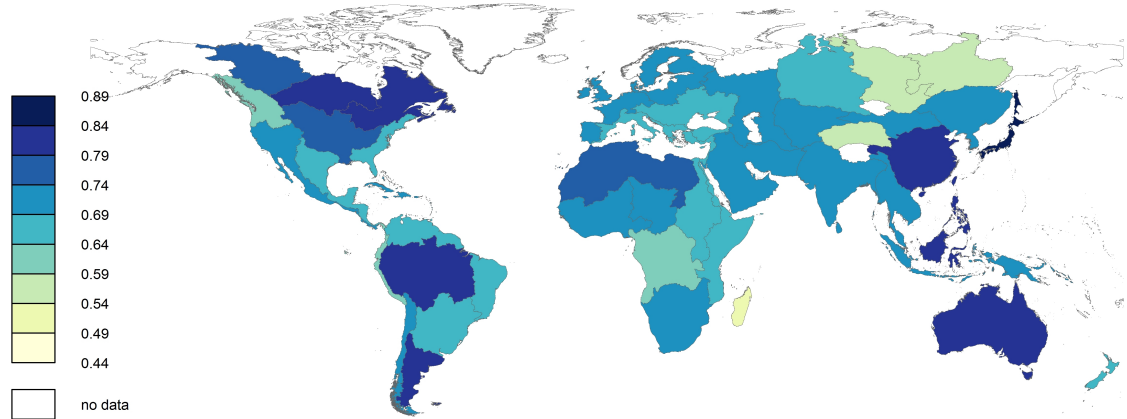


Figure 5. World map of the area under the receiver operating characteristic curve (AUC) for the globally-fitted random forest model. The AUC is evaluated using out-of-sample observations aggregated over each level 2 watershed (HS2) and indicates the probability that a model can differentiate between “flood” and “no flood”.

461 In the Supporting Information, we present the ROC curve and other validation measures
 462 used to support these results.

463 Figure 5 demonstrates the performance of the globally fitted random forest in terms
 464 of the area under the ROC curve aggregated over HS2 watersheds. The occurrence model
 465 does particularly well in Eastern Canada, Eastern China, Japan, Indonesia, Australia,
 466 and the Amazon. The global random forest model shows predictive skill (AUC more than
 467 0.5) over all regional HS2 watersheds, and generally has the ability to identify the
 468 environmental and socioeconomic features that generate flood occurrence. We are encour-
 469 aged that only 6 of the 62 HS2 watersheds have an AUC less than 0.6.

470 Table 5 lists the 10 most significant predictors found to explain flood occurrence
 471 with the globally fitted RF model. Regardless of the measure chosen, the two exposure
 472 predictors of GDP per capita and population density are prominent. Unsurprisingly, the
 473 precipitation over various timescales are key predictors. Annual mean temperature is also
 474 an important predictor, driven by its link to interannual patterns in evapotranspiration.
 475 The remaining predictors represent the residual components of flood hydrology. Topo-
 476 graphic effects are represented by the topographic position index and aspect, soil con-
 477 tent by gravel, and land usage by cropland. Bedrock porosity provides a proxy of longer
 478 term storage.

479 4.2 Impact

480 As with the occurrence model, we fit each model globally and by HS2 regional sub-
 481 sets of watersheds. In terms of the quality of the out-of-sample fit, we again cannot claim
 482 that the NN models outperform the others, so given their complexity we do not recom-
 483 mend them. Linear models (LM) perform poorly globally but their fit improve once fit-
 484 ted over different subsets of watersheds (Table 6). However, LM are outperformed by
 485 RF in terms of global and local fit and hence we recommend the latter method for this
 486 application. The Supporting Information presents the RMSE and R^2 for all three mod-
 487 els fit globally and by regional subsets of watersheds.

RMSE RF

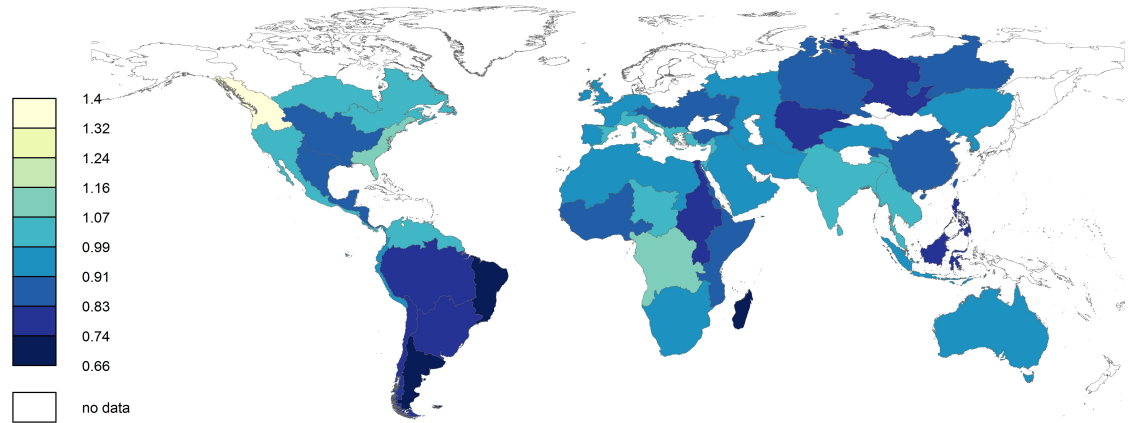


Figure 6. World map of the out-of-sample RMSE for each level 2 watershed for the globally fitted random forest model.

R2 RF

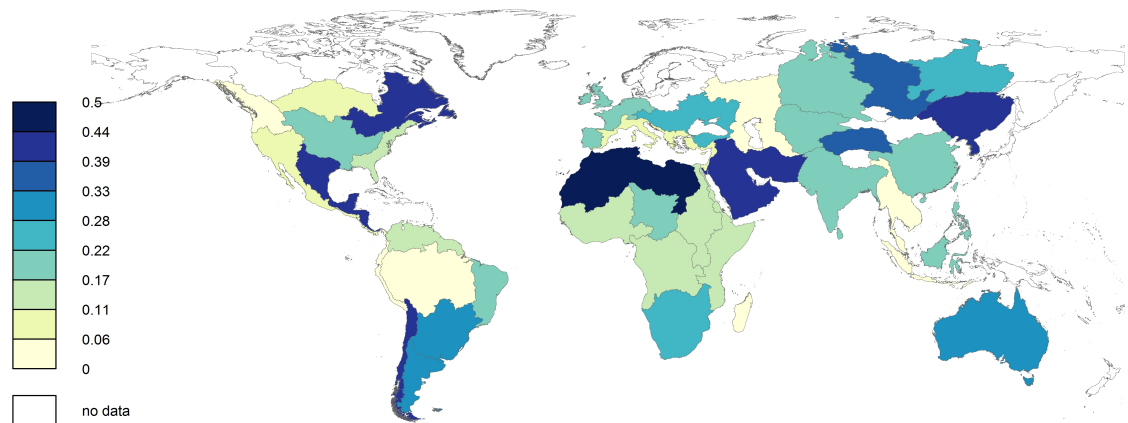


Figure 7. World map of the out-of-sample R-squared for each level 2 watershed for the globally fitted random forest model.

Figure 6 shows the root-mean-square error (RMSE) aggregated by HS2 watershed regions for the random forest fitted globally. Almost all HS2 regions have an out-of-sample RMSE below 1, which given the log10 scale of the fraction of population displaced used as the response variable, indicates that the predictions are within an order of magnitude of the observations. This result is excellent given that impact ranges over 8 orders of magnitude (Figure 4b). It is also important to note that in the observations, the fraction of displaced people is very small (mainly in the range of $[-5, -2]$ on a log10 scale) meaning that absolute errors, rather than relative errors, are quite small. Moreover, only one quarter of the HS2 watersheds analyzed have an out-of-sample R^2 below 10%, while the majority are above 20% (Figure 7) and many of them are above 40%. Given the challenge of predicting the fraction of the population affected by a flood over the globe, we find these to be promising results. A number of the poorer predictive results are influenced by limited observations, such as for Madagascar, Papua New Guinea, and New Zealand (see Supporting Information). However, for the more challenging watersheds the predictors are not representing the fraction displaced because 1. other predictors represent the relevant flood regimes in those watersheds, 2. there are biases or inaccuracies in the impact observations, 3. there are biases in the manner in which the persons displaced are associated to particular watersheds. For the impact model, we are reassured by good levels of out-of-sample variance explained over the majority of the globe, and by a lack of systemic patterns in the watersheds with poorer variance explained.

Table 7 lists the 10 most significant predictors in the globally fitted random forest impact model. Regardless of the measure used, we find that most timescales of precipitation and temperature variables need to be included in the model, as well as population density and GDP per capita. The resulting predictors are similar to those identified in the occurrence model, with lagged temperature predictors taking on an important explicative role. Overall, we find that lagged precipitation and temperature variables, when applied with the exposure predictors of GDP per capita and population density, capture the majority of the resolved signal of seasonal flooding.

4.3 Global Model

This section assesses the entire flood catalogue, which consists of 1 million simulated years of flood occurrences and impacts over 4734 watersheds globally. We first evaluate the displaced fraction of population and then the simulated occurrence and population displaced. Despite the bias correction of precipitation and temperature, the time-varying CESM-LE output and basin-scale predictors do not sufficiently capture impact extremes. This results in underestimated densities for both low and high values of the fraction displaced (Supporting Information). To remedy this issue in a simple way, we scaled the standard deviation parameters of the impact distribution to match the observed standard deviation (Supporting Information).

Figure 8 compares the mean simulated and observed occurrence and impact aggregated over level 3 watersheds (HS3). It is important to note that such a comparison is ambitious since the performance of the global model depends on the performance of the CESM-LE to generate conditions favorable for flood. As such, the clustering of points along the 45° lines indicates that the global model works well overall to simulate a realistic number of floods and displaced people compared to the observations. For low risk areas though, the model tends to slightly overestimate flood hazard. This could be because no flood was observed over the 32-year observational record even if the true flood probability is non-zero. This bias results in overestimates of the number of displaced people for small population watersheds. Nevertheless, for HS3 watersheds with an annual mean of more than 300 people displaced (the great majority of basins where risk analysis is relevant), the model predictions fit the observations well.

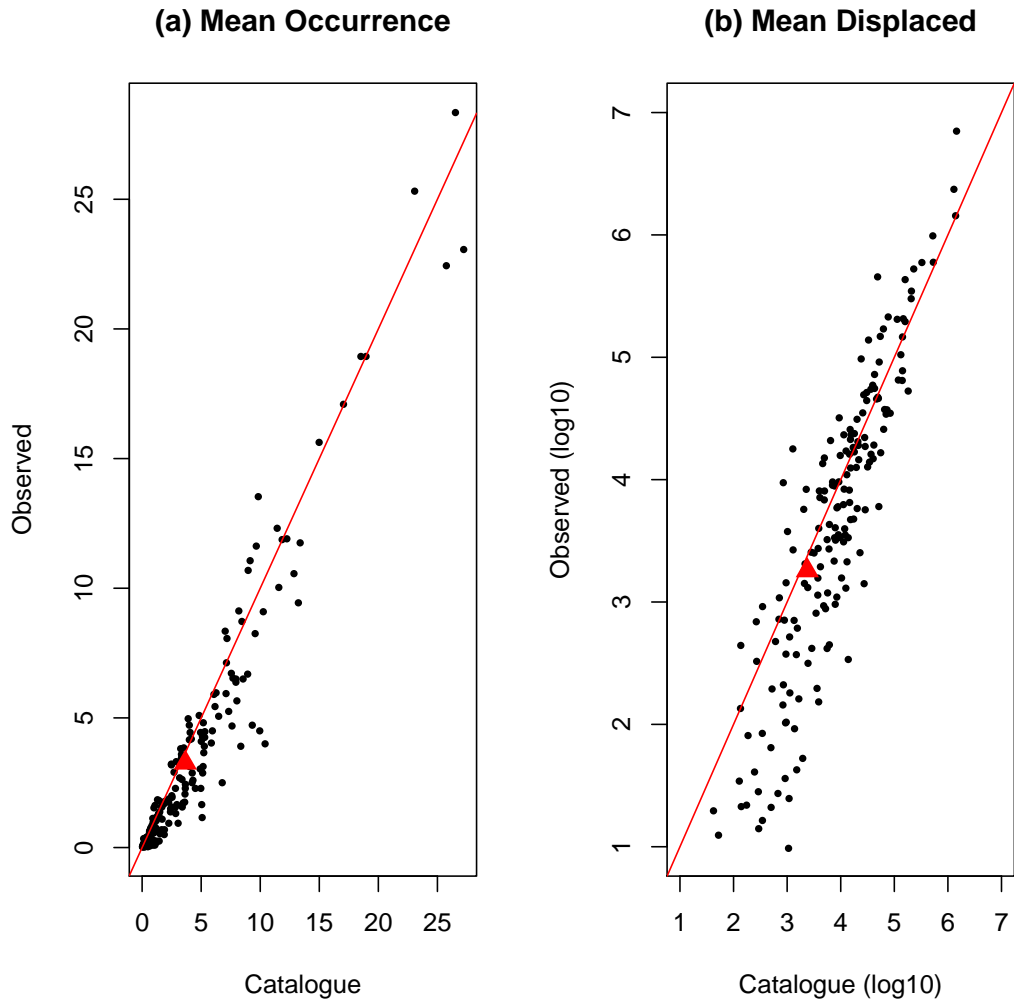


Figure 8. Observed versus simulated flood occurrence and population displaced aggregated by level 3 watersheds. (a) Mean observed flood frequency versus mean simulated frequency. (b) Mean observed versus simulated population displaced, expressed on a log10 scale. The red triangle represents the mean. Averages of observations are taken over the 32 hydrological years available from the DFO and over 1 million years for the catalogue.

HS3 log10 displaced error

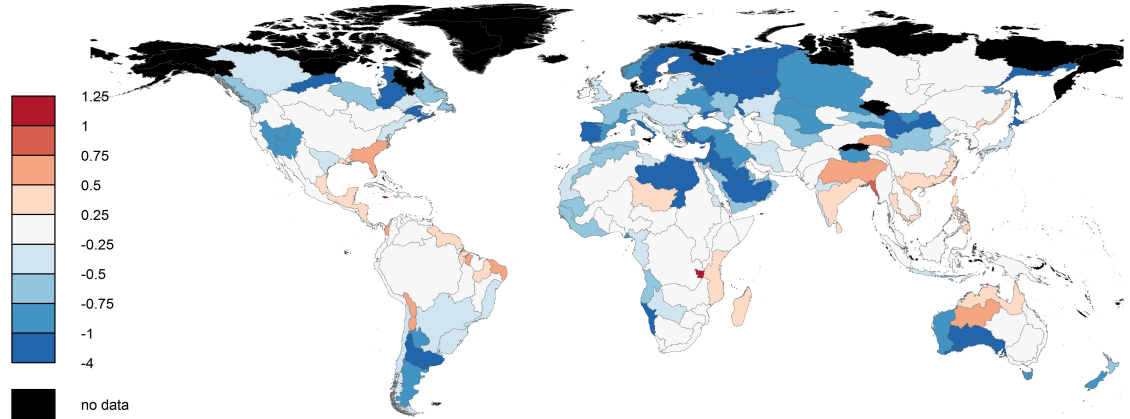


Figure 9. World map of the error on the mean number of displaced people. Represented as the mean observed displaced population less the mean displaced population in the catalog (with each member of the difference being on a log10 scale). Negative values indicate the model overestimates observations.

538 The world map in Figure 9 illustrates the average error in the number of displaced
 539 people. The darkest blue shade represents locations where the overestimation is larger
 540 than a factor of 10. Of these regions, we observe that they are either in far northern re-
 541 gions (Northern Canada, Sweden, Finland, North-Western Russia) or dry climates (Libya,
 542 Egypt, Saudi Arabia, and Southwest Australia). While flood is not common in these re-
 543 gions, biases could be due to underreporting in DFO in these regions as they are sparsely
 544 populated, to overestimates in the CESM-LE flood-generating conditions, or a lack of
 545 fit of the occurrence/impact statistical models due to a lack of observations. Looking back
 546 to Figures 5 and 7, the fit of both statistical models is good in dry climates but not as
 547 successful over northern regions. Overall, there are less cases of underestimated popu-
 548 lation displaced. The model underestimates population displaced in a few South Asian
 549 watersheds in Bangladesh, India, and Nepal. This region, particularly Bangladesh, is known
 550 for extreme floods resulting in millions of displaced driven by the unique combination
 551 of precipitation extremes from the annual Indian Monsoon, low-lying and complex hy-
 552 drology, high population, and poor infrastructure (Dewan, 2015), which is beyond the
 553 ability of our model to capture.

554 5 Applications

555 To illustrate potential uses for the model, we show global flood hazard and risk maps
 556 based on the stochastic catalogue comprised of one million years of events. Flood haz-
 557 ard is expressed as the annual flood probability whereas flood risk combines flood haz-
 558 ard with population and wealth exposed.

559 Figure 10 presents the annual mean flood frequency in the catalogue for each HS5
 560 watershed, which can be interpreted as the annual flood probability over each HS5 wa-
 561 tershed. Darker colors point to flood hot spots, with the highest flood probabilities in
 562 northeastern India, Bangladesh, and Myanmar being driven by the annual South Asian
 563 monsoons. Southeastern China, Japan, and certain areas of Southeast Asia are also high
 564 hazard areas. Other regional peaks are found in eastern USA, southern Mexico and Cen-

Flood hazard

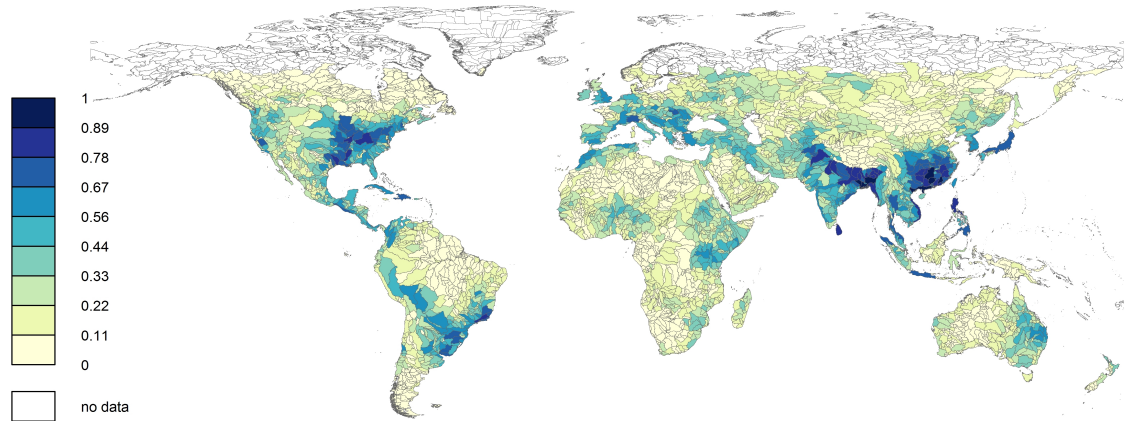


Figure 10. Global flood hazard map by level 5 watershed expressed as the annual flood probability.

Flood risk - Population displaced (log10)

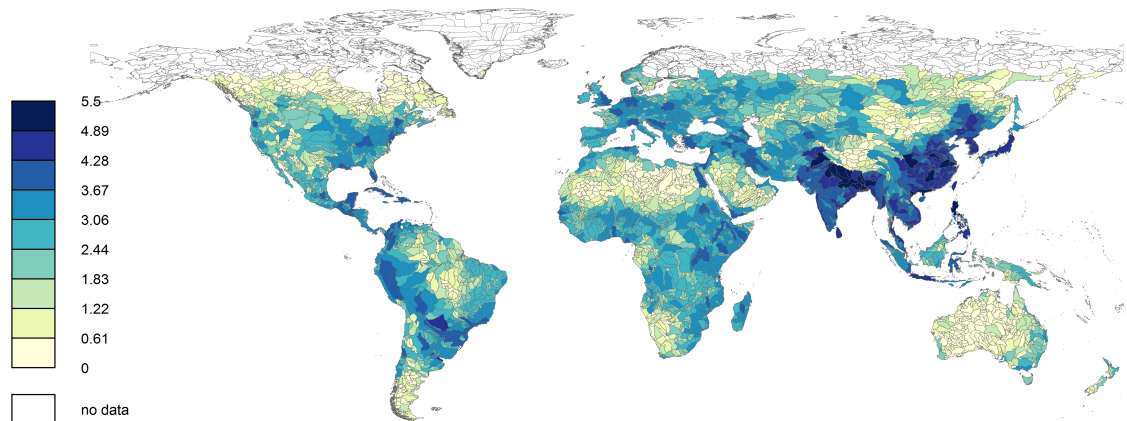


Figure 11. Global flood risk map, expressed as the average population displaced (log10).

565 tral America, southern Brazil, and parts of Europe. Although these probabilities seem
 566 high, they represent the likelihood that at least one river within an HS5 watershed over-
 567 flows sufficiently so that a minimum number of people are displaced. It should not be
 568 compared to typical return periods.

569 The annual average population displaced over each HS5 watershed (Figure 11) com-
 570 bines flood hazard (flood probability) and exposure (population) to yield the average num-
 571 ber of displaced people in any given year (flood risk). For example, over Northern In-
 572 dia, Bangladesh and China, many highly densely populated watersheds yield an annual
 573 average number of displaced people of over 100,000. Over Central Europe, for example,
 574 many watersheds have an average annual number of displaced people of about 1,000. We
 575 expect this model of flood risk to be highly relevant to risk management and socioeco-
 576 nomic studies.

Flood Risk - GDP Affected (log10)

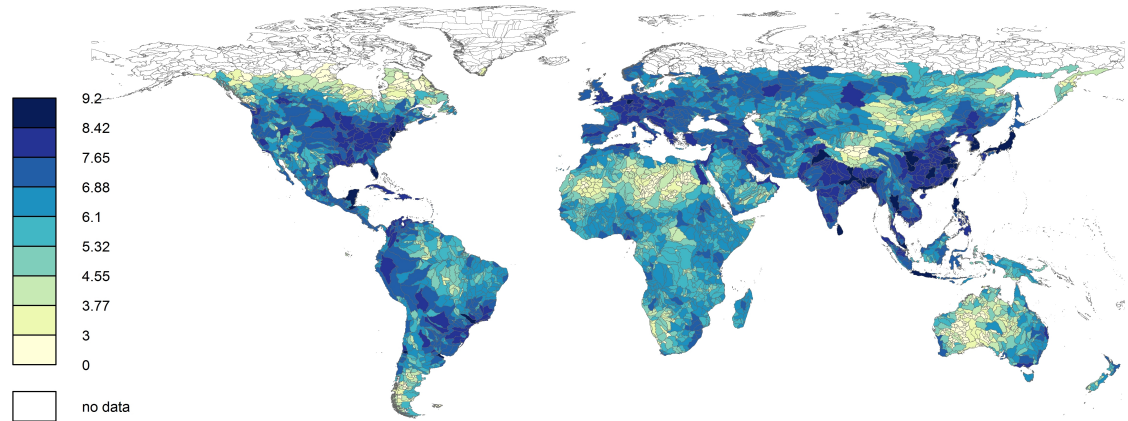


Figure 12. Global flood risk map, expressed as the average GDP produced by the displaced population (log10, US dollars)

577 To illustrate the global scale economic loss potential of flood, we translate popu-
 578 lation displaced into the GDP of the population displaced by simply multiplying by the
 579 annual GDP per capita (Kummu et al., 2018). Figure 12 presents this alternative per-
 580 spective of flood risk, with exposure being the GDP of the population over a given wa-
 581 tershed. This view of flood risk is more targeted to studies of economic loss and finan-
 582 cial risk management. In terms of GDP affected, less developed high population water-
 583 sheds remain important, yet hot spots appear in wealthier regions in Europe (UK, East
 584 of France, Belgium, Netherlands, Germany, and Italy), North America (Eastern USA and
 585 West Coast USA, Southern Canada), South America (Southern Brazil and Northeast-
 586 ern Argentina), and Australia (Brisbane and Melbourne).

587 6 Conclusion

588 By integrating the Dartmouth Flood Observatory database of historical flood events
 589 with the HydroBASINS database of watersheds, we created novel flood occurrence and
 590 impact databases that describe flood frequency and intensity over a watershed in terms
 591 of the climatic, watershed, and socioeconomic drivers. We then fitted classical regres-
 592 sion and machine learning techniques to these data, and adopted the random forest model
 593 fitted to observations at the global scale. Finally, we generated a global catalogue of flood
 594 events by forcing the empirical model with bias-corrected precipitation and temperature
 595 output from the large ensemble of the NCAR CESM climate model.

596 The unique value of this global flood model lies in its ability to quickly simulate
 597 realistic flood events at a resolution that is useful for large-scale socioeconomic and fi-
 598 nancial planning. Translating outputs from a climate model into flood events facilitates
 599 the creation of scenarios and projections of impacts over various time horizons. One could
 600 apply global weather or seasonal forecasts to simulate flood impacts over time horizons
 601 from days to months, or focus on different time horizons from the NCAR CESM climate
 602 model and investigate the impacts of climate change on flood hazard and risk. Alternat-
 603 ively, subsets of the catalogue could be extracted to investigate the impacts of various
 604 climate oscillations on flood hazard and various measures of risk. Including population
 605 and wealth per capita in the model allows for sensitivity testing and experimentation of

the dependence of flood hazard and risk to changes in the spatial population and wealth patterns. Finally, one could conveniently consider shocks to the outputs of the climate model (such as significant changes in precipitation over a given area in a year) and evaluate different climate scenarios, as will be required by regulators of the financial services industry. We expect this model to be a useful empirically-based though climatically-consistent complement to the mechanistic and other approaches available.

Acknowledgments

The data used in our model development is detailed in section 2. The HydroBASINS dataset is available at <https://www.hydrosheds.org/>. The Dartmouth Flood Observatory (DFO) Global Active Archive of Large Flood Events can be downloaded at <https://floodobservatory.colorado.edu/Archives/index.html>. The CHIRPS global precipitation dataset can be downloaded at <https://doi.org/10.15780/G2RP4Q>. CPC Global Temperature data provided by the NOAA/OAR/ESRL PSD, Boulder, Colorado, USA, from their Web site at <https://www.esrl.noaa.gov/psd/data/gridded/data.cpc.globaltemp.html>. CPC Global Unified Precipitation data provided by the NOAA/OAR/ESRL PSD, Boulder, Colorado, USA, from their Web site at <https://www.esrl.noaa.gov/psd/>. The High-resolution global topographic index (TI) dataset is available at <https://doi.org/10.5285/6b0c4358-2bf3-4924-aa8f-793d468b92be>. The Global Soil Dataset for Earth System Modeling (GSD) can be downloaded at <http://globalchange.bnu.edu.cn/research/soilw>. The Global Depth to Bedrock Dataset for Earth System Modeling is available at <http://globalchange.bnu.edu.cn/research/dtb.jsp>. The GLobal HYdrogeology MaPS data is available at <https://doi.org/10.5683/SP2/TTJNIU>. The FAO Global Land Cover (GLC-SHARE) Beta-Release 1.0 database available at <http://www.fao.org/land-water/land/land-governance/land-resources-planning-toolbox/category/details/en/c/1036355/>. The Gridded Population of the World (GPW) Version 4 Release 11 population count data is available at <https://sedac.ciesin.columbia.edu/data/set/gpw-v4-population-count-rev11>. The Anthropogenic land-use estimates for the Holocene; HYDE 3.2 dataset is available at <https://doi.org/10.17026/dans-25g-gez3>. Gridded global datasets for Gross Domestic Product and Human Development Index (GDPHDI) over 1990-2015 are available at <https://doi.org/10.5061/dryad.dk1j0>. The CESM Large Ensemble dataset is available at <https://www.earthsystemgrid.org/> and the authors acknowledge CESM Large Ensemble Community Project and supercomputing resources provided by NSF/CISL/Yellowstone. The data supplement to this article is available at <https://doi.org/10.5281/zenodo.3873422> and contains datasets, fitted statistical models, and an analysis script (Carozza & Boudreault, 2020).

This work was supported by Mitacs through the Mitacs Accelerate program. This work was partially funded by AXA XL, the property & casualty and specialty risk division of AXA. We acknowledge the support of the Fonds de recherche du Québec – Nature et technologies (FRQNT), [funding reference number 119908]. Cette recherche a été financée par le Fonds de recherche du Québec – Nature et technologies (FRQNT), [numéro de référence 119908]. We acknowledge the support of the Natural Sciences and Engineering Research Council of Canada (NSERC), [funding reference number PDF-502939-2017]. Cette recherche a été financée par le Conseil de recherches en sciences naturelles et en génie du Canada (CRSNG), [numéro de référence PDF-502939-2017].

Both authors contributed equally to this work.

The authors declare that there is no conflict of interest regarding the publication of this article.

The authors would like to thank Tom Philp from AXA-XL for his support and feedback on this work, Robert Erhardt for discussions on the model methodology, and Manuel Grenier for comments on the manuscript.

References

656

657 Bank of England. (2019). *The 2021 biennial exploratory scenario on the financial*
 658 *risks from climate change*. Bank of England.

659 Barredo, J. I. (2009). Normalised flood losses in europe: 1970–2006. *Natural Hazards*
 660 *and Earth System Sciences*, 9(1), 97–104. Retrieved from [https://www.nat-](https://www.nat-hazards-earth-syst-sci.net/9/97/2009/)
 661 [-hazards-earth-syst-sci.net/9/97/2009/](https://www.nat-hazards-earth-syst-sci.net/9/97/2009/) doi: 10.5194/nhess-9-97-2009

662 Barthel, F., & Neumayer, E. (2011, Dec). A trend analysis of normalized insured
 663 damage from natural disasters. *Climatic Change*, 113(2), 215–237. Retrieved
 664 from [http://dx.doi.org/10.1007/s10584-](http://dx.doi.org/10.1007/s10584-011-0331-2)
 665 [-011-0331-2](http://dx.doi.org/10.1007/s10584-011-0331-2) doi: 10.1007/s10584

666 Bergmeir, C., & Benítez, J. M. (2012). Neural networks in R using the stuttgart
 667 neural network simulator: RSNNS. *Journal of Statistical Software*, 46(7), 1–
 668 26. Retrieved from <http://www.jstatsoft.org/v46/i07/>

669 Bevin, K. (2012). Down to basics: Runoff processes and the modelling process. In
 670 *Rainfall-runoff modelling* (p. 1-23). John Wiley & Sons, Ltd. Retrieved from
 671 <https://onlinelibrary.wiley.com/doi/abs/10.1002/9781119951001.ch1>
 672 doi: 10.1002/9781119951001.ch1

673 Brakenridge, G. (2010). *Global active archive of large flood events*. Dart-
 674 mouth Flood Observatory, University of Colorado. Retrieved from [http://](http://floodobservatory.colorado.edu/Archives/index.html)
 675 floodobservatory.colorado.edu/Archives/index.html (Accessed: 2018-5-
 676 22)

677 Breiman, L. (2001). Random forests. *Machine Learning*, 45(1), 5–32. doi: 10.1023/
 678 A:1010933404324

679 Carozza, D. A., & Boudreault, M. (2020, June). *A global flood risk modeling frame-*
 680 *work built with climate models and machine learning - Submission - Data Sup-*
 681 *plement*. Zenodo. Retrieved from <https://doi.org/10.5281/zenodo.3873422>
 682 doi: 10.5281/zenodo.3873422

683 CIESIN. (2018). *Gridded Population of the World, Version 4 (GPWv4): Population*
 684 *Count, Revision 11*. Palisades, NY: NASA Socioeconomic Data and Applica-
 685 tions Center (SEDAC). (Accessed: 2019-11-22) doi: 10.7927/H4JW8BX5

686 de Bruijn, K. M., Diermanse, F. L. M., & Beckers, J. V. L. (2014). An advanced
 687 method for flood risk analysis in river deltas, applied to societal flood fatality
 688 risk in the netherlands. *Natural Hazards and Earth System Sciences*, 14(10),
 689 2767–2781. Retrieved from [https://www.nat-hazards-earth-syst-sci.net/](https://www.nat-hazards-earth-syst-sci.net/14/2767/2014/)
 690 [14/2767/2014/](https://www.nat-hazards-earth-syst-sci.net/14/2767/2014/) doi: 10.5194/nhess-14-2767-2014

691 Dewan, T. H. (2015). Societal impacts and vulnerability to floods in bangladesh and
 692 nepal. *Weather and Climate Extremes*, 7, 36 - 42. Retrieved from [http://www](http://www.sciencedirect.com/science/article/pii/S2212094714000930)
 693 [.sciencedirect.com/science/article/pii/S2212094714000930](http://www.sciencedirect.com/science/article/pii/S2212094714000930) (SI: IGBP
 694 APN) doi: <https://doi.org/10.1016/j.wace.2014.11.001>

695 Dottori, F., Szewczyk, W., Ciscar, J.-C., Zhao, F., Alfieri, L., Hirabayashi, Y., ...
 696 et al. (2018, Aug). Increased human and economic losses from river flood-
 697 ing with anthropogenic warming. *Nature Climate Change*, 8(9), 781–786.
 698 Retrieved from <http://dx.doi.org/10.1038/s41558-018-0257-z> doi:
 699 [10.1038/s41558-018-0257-z](http://dx.doi.org/10.1038/s41558-018-0257-z)

700 Dowle, M., & Srinivasan, A. (2018). data.table: Extension of ‘data.frame’ [Com-
 701 puter software manual]. Retrieved from [https://CRAN.R-project.org/](https://CRAN.R-project.org/package=data.table)
 702 [package=data.table](https://CRAN.R-project.org/package=data.table) (R package version 1.11.8)

703 Doxsey-Whitfield, E., MacManus, K., Adamo, S. B., Pistolesi, L., Squires, J.,
 704 Borkovska, O., & Baptista, S. R. (2015). Taking advantage of the im-
 705 proved availability of census data: A first look at the gridded population
 706 of the world, version 4. *Papers in Applied Geography*, 1(3), 226-234. doi:
 707 [10.1080/23754931.2015.1014272](https://doi.org/10.1080/23754931.2015.1014272)

708 Falter, D., Dung, N., Vorogushyn, S., Schröter, K., Hundecha, Y., Kreibich, H.,
 709 ... Merz, B. (2016). Continuous, large-scale simulation model for flood risk
 710 assessments: proof-of-concept. *Journal of Flood Risk Management*, 9(1), 3-

- 711 21. Retrieved from [https://onlinelibrary.wiley.com/doi/abs/10.1111/](https://onlinelibrary.wiley.com/doi/abs/10.1111/jfr3.12105)
712 [jfr3.12105](https://onlinelibrary.wiley.com/doi/abs/10.1111/jfr3.12105) doi: 10.1111/jfr3.12105
- 713 Farr, T. G., Rosen, P. A., Caro, E., Crippen, R., Duren, R., Hensley, S., ... Alsdorf,
714 D. (2007). The shuttle radar topography mission. *Reviews of Geophysics*,
715 *45*(2). Retrieved from [https://agupubs.onlinelibrary.wiley.com/doi/](https://agupubs.onlinelibrary.wiley.com/doi/abs/10.1029/2005RG000183)
716 [abs/10.1029/2005RG000183](https://agupubs.onlinelibrary.wiley.com/doi/abs/10.1029/2005RG000183) doi: 10.1029/2005RG000183
- 717 Fawcett, T. (2006). An introduction to roc analysis. *Pattern Recognition Letters*,
718 *27*(8), 861 - 874. (ROC Analysis in Pattern Recognition) doi: [https://doi.org/](https://doi.org/10.1016/j.patrec.2005.10.010)
719 [10.1016/j.patrec.2005.10.010](https://doi.org/10.1016/j.patrec.2005.10.010)
- 720 FRBSF. (2019). Strategies to address climate change risk in low- and moderate-
721 income communities. *Federal Reserve Bank of San Francisco Community De-*
722 *velopment Innovation Review*, *14*, 001–168. doi: 10.24148/cdir2019-01
- 723 Funk, C. (2015). *CHIRPS v2.0*. Climate Hazards Group. doi: 10.15780/G2RP4Q
- 724 Funk, C., Peterson, P., Landsfeld, M., Pedreros, D., Verdin, J., Shukla, S., ...
725 Michaelsen, J. (2015). The climate hazards infrared precipitation with sta-
726 tions—a new environmental record for monitoring extremes. *Scientific Data*.
- 727 Gall, M., Borden, K. A., & Cutter, S. L. (2009). When do losses count? *Bulletin of*
728 *the American Meteorological Society*, *90*(6), 799-810. Retrieved from [https://](https://doi.org/10.1175/2008BAMS2721.1)
729 doi.org/10.1175/2008BAMS2721.1 doi: 10.1175/2008BAMS2721.1
- 730 Giraud, T., & Lambert, N. (2016, aug). cartography: Create and integrate maps in
731 your r workflow. *The Journal of Open Source Software*, *1*(4). Retrieved from
732 <http://dx.doi.org/10.21105/joss.00054> doi: 10.21105/joss.00054
- 733 Gleeson, T., Moosdorf, N., Hartmann, J., & van Beek, L. P. H. (2014). A glimpse
734 beneath earth's surface: Global hydrogeology maps (glhymps) of permeability
735 and porosity. *Geophysical Research Letters*, *41*(11), 3891-3898. (Accessed data:
736 2018-5-7) doi: 10.1002/2014GL059856
- 737 Gruber, A., Scanlon, T., van der Schalie, R., Wagner, W., & Dorigo, W. (2019).
738 Evolution of the esa cci soil moisture climate data records and their under-
739 lying merging methodology. *Earth System Science Data*, *11*(2), 717–739.
740 Retrieved from <https://www.earth-syst-sci-data.net/11/717/2019/> doi:
741 [10.5194/essd-11-717-2019](https://www.earth-syst-sci-data.net/11/717/2019/)
- 742 Hastie, T., Tibshirani, R., & Friedman, J. (2009). *The Elements of Statistical Learn-*
743 *ing*. Springer New York. doi: 10.1007/978-0-387-84858-7
- 744 Hempel, S., Frieler, K., Warszawski, L., Schewe, J., & Piontek, F. (2013). A trend-
745 preserving bias correction; the isi-mip approach. *Earth System Dynamics*,
746 *4*(2), 219–236. Retrieved from [https://www.earth-syst-dynam.net/4/219/](https://www.earth-syst-dynam.net/4/219/2013/)
747 [2013/](https://www.earth-syst-dynam.net/4/219/2013/) doi: 10.5194/esd-4-219-2013
- 748 Hrachowitz, M., Savenije, H., Blöschl, G., McDonnell, J., Sivapalan, M., Pomeroy,
749 J., ... Cudennec, C. (2013). A decade of predictions in ungauged basins
750 (pub)—a review. *Hydrological Sciences Journal*, *58*(6), 1198-1255. Re-
751 trieved from <https://doi.org/10.1080/02626667.2013.803183> doi:
752 [10.1080/02626667.2013.803183](https://doi.org/10.1080/02626667.2013.803183)
- 753 Hu, P., Zhang, Q., Shi, P., Chen, B., & Fang, J. (2018). Flood-induced mortal-
754 ity across the globe: Spatiotemporal pattern and influencing factors. *Sci-*
755 *ence of The Total Environment*, *643*, 171 - 182. Retrieved from [http://](http://www.sciencedirect.com/science/article/pii/S0048969718322745)
756 www.sciencedirect.com/science/article/pii/S0048969718322745 doi:
757 <https://doi.org/10.1016/j.scitotenv.2018.06.197>
- 758 Hunziker, P. (2017). *velox: Fast raster manipulation and extraction [Computer soft-*
759 *ware manual]*. Retrieved from <https://CRAN.R-project.org/package=velox>
760 (R package version 0.2.0)
- 761 Hurrell, J. W., Holland, M. M., Gent, P. R., Ghan, S., Kay, J. E., Kushner, P. J.,
762 ... Marshall, S. (2013). The community earth system model: A framework for
763 collaborative research. *Bulletin of the American Meteorological Society*, *94*(9),
764 1339-1360. Retrieved from <https://doi.org/10.1175/BAMS-D-12-00121.1>
765 doi: 10.1175/BAMS-D-12-00121.1

- 766 Jongman, B., Hochrainer-Stigler, S., Feyen, L., Aerts, J. C. J. H., Mechler, R.,
767 Botzen, W. J. W., ... Ward, P. J. (2014, Mar). Increasing stress on
768 disaster-risk finance due to large floods. *Nature Climate Change*, 4(4),
769 264–268. Retrieved from <http://dx.doi.org/10.1038/nclimate2124> doi:
770 10.1038/nclimate2124
- 771 Jongman, B., Ward, P. J., & Aerts, J. C. (2012). Global exposure to river and
772 coastal flooding: Long term trends and changes. *Global Environmental*
773 *Change*, 22(4), 823 - 835. Retrieved from [http://www.sciencedirect.com/](http://www.sciencedirect.com/science/article/pii/S0959378012000830)
774 [science/article/pii/S0959378012000830](http://www.sciencedirect.com/science/article/pii/S0959378012000830) doi: [https://doi.org/10.1016/](https://doi.org/10.1016/j.gloenvcha.2012.07.004)
775 [j.gloenvcha.2012.07.004](https://doi.org/10.1016/j.gloenvcha.2012.07.004)
- 776 Kay, J. E., Deser, C., Phillips, A., Mai, A., Hannay, C., Strand, G., ... Vertenstein,
777 M. (2015, August). The Community Earth System Model (CESM) Large
778 Ensemble Project: A Community Resource for Studying Climate Change
779 in the Presence of Internal Climate Variability. *Bulletin of the American*
780 *Meteorological Society*, 96, 1333-1349. (Data accessed: 2018-6-29) doi:
781 10.1175/BAMS-D-13-00255.1
- 782 Klein Goldewijk, K. (2017). *Anthropogenic land-use estimates for the Holocene;*
783 *HYDE 3.2*. Data Archiving and Networked Services (DANS). (Accessed: 2020-
784 01-17) doi: 10.17026/DANS-25G-GEZ3
- 785 Klein Goldewijk, K., Beusen, A., Doelman, J., & Stehfest, E. (2017). Anthropogenic
786 land use estimates for the holocene – hyde 3.2. *Earth System Science Data*,
787 9(2), 927–953. doi: 10.5194/essd-9-927-2017
- 788 Kumm, M., Taka, M., & Guillaume, J. H. A. (2018). Gridded global datasets for
789 gross domestic product and human development index over 1990–2015. *Scien-*
790 *tific Data*, 5(180004). doi: 10.1038/sdata.2018.4
- 791 Kumm, M., Taka, M., & Guillaume, J. H. A. (2019). *Gridded global datasets for*
792 *Gross Domestic Product and Human Development Index over 1990-2015, v2*.
793 Dryad, Dataset. (Accessed: 2018-11-14) doi: 10.5061/dryad.dk1j0
- 794 Latham, J., Cumani, R., Rosati, I., & Bloise, M. (2014). FAO Global Land Cover
795 (GLC-SHARE) Beta-Release 1.0 Database. *FAO Land and Water Division*.
796 (Accessed data: 2018-3-30)
- 797 Lawrence, D. M., Oleson, K. W., Flanner, M. G., Thornton, P. E., Swenson, S. C.,
798 Lawrence, P. J., ... Slater, A. G. (2011). Parameterization improvements
799 and functional and structural advances in version 4 of the community land
800 model. *Journal of Advances in Modeling Earth Systems*, 3(1). Retrieved
801 from [https://agupubs.onlinelibrary.wiley.com/doi/abs/10.1029/](https://agupubs.onlinelibrary.wiley.com/doi/abs/10.1029/2011MS00045)
802 [2011MS00045](https://agupubs.onlinelibrary.wiley.com/doi/abs/10.1029/2011MS00045) doi: 10.1029/2011MS00045
- 803 Lehner, B., & Grill, G. (2013). Global river hydrography and network routing: base-
804 line data and new approaches to study the world's large river systems. *Hydro-*
805 *logical Processes*, 27(15), 2171-2186. (Data accessed: 2018-4-20) doi: 10.1002/
806 hyp.9740
- 807 Li, S., Kang, S., Zhang, L., Zhang, J., Du, T., Tong, L., & Ding, R. (2016). Evalu-
808 ation of six potential evapotranspiration models for estimating crop potential
809 and actual evapotranspiration in arid regions. *Journal of Hydrology*, 543, 450 -
810 461. doi: <https://doi.org/10.1016/j.jhydrol.2016.10.022>
- 811 Liaw, A., & Wiener, M. (2002). Classification and regression by randomforest.
812 *R News*, 2(3), 18-22. Retrieved from [https://CRAN.R-project.org/doc/](https://CRAN.R-project.org/doc/Rnews/)
813 [Rnews/](https://CRAN.R-project.org/doc/Rnews/)
- 814 Marthews, T., Dadson, S., Lehner, B., Abele, S., & Gedney, N. (2015a). *High-*
815 *resolution global topographic index values*. NERC Environmental Information
816 Data Centre. (Accessed: 2018-8-6) doi: 10.5285/6b0c4358-2bf3-4924-aa8f
817 -793d468b92be
- 818 Marthews, T., Dadson, S. J., Lehner, B., Abele, S., & Gedney, N. (2015b). High-
819 resolution global topographic index values for use in large-scale hydrologi-
820 cal modelling. *Hydrology and Earth System Sciences*, 19(1), 91–104. doi:

- 821 10.5194/hess-19-91-2015
- 822 McCulloch, W. S., & Pitts, W. (1943). A logical calculus of the ideas immanent in
823 nervous activity. *The Bulletin of Mathematical Biophysics*, 5(4), 115–133. doi:
824 10.1007/BF02478259
- 825 Meløysund, V., Leira, B., Høiset, K. V., & Lisø, K. R. (2007). Predicting snow
826 density using meteorological data. *Meteorological Applications*, 14(4), 413–
827 423. Retrieved from [https://rmets.onlinelibrary.wiley.com/doi/abs/](https://rmets.onlinelibrary.wiley.com/doi/abs/10.1002/met.40)
828 [10.1002/met.40](https://rmets.onlinelibrary.wiley.com/doi/abs/10.1002/met.40) doi: 10.1002/met.40
- 829 Microsoft, C., & Weston, S. (2017). dosnow: Foreach parallel adaptor for the
830 'snow' package [Computer software manual]. Retrieved from [https://](https://CRAN.R-project.org/package=doSNOW)
831 CRAN.R-project.org/package=doSNOW (R package version 1.0.16)
- 832 Munoz, S. E., & Dee, S. G. (2017, May). El niño increases the risk of lower missis-
833 sippi river flooding. *Scientific Reports*, 7(1). doi: 10.1038/s41598-017-01919-6
- 834 Neale, R., Chen, C.-C., & Gettelman, A. (2012). Description of the near community
835 atmosphere model (cam5), technical report near/tn-486+st. *National Center*
836 *for Atmospheric Research, Boulder, Colorado*, 268. Retrieved from [https://](https://doi.org/10.1175/1520-0469(1999)056<0642:TOSEOT>2.0.CO;2)
837 [doi.org/10.1175/1520-0469\(1999\)056<0642:TOSEOT>2.0.CO;2](https://doi.org/10.1175/1520-0469(1999)056<0642:TOSEOT>2.0.CO;2)
- 838 Neumayer, E., & Barthel, F. (2011). Normalizing economic loss from natural
839 disasters: A global analysis. *Global Environmental Change*, 21(1), 13 - 24.
840 Retrieved from [http://www.sciencedirect.com/science/article/pii/](http://www.sciencedirect.com/science/article/pii/S0959378010001019)
841 [S0959378010001019](http://www.sciencedirect.com/science/article/pii/S0959378010001019) doi: <https://doi.org/10.1016/j.gloenvcha.2010.10.004>
- 842 Neuwirth, E. (2014). Rcolorbrewer: Colorbrewer palettes [Computer software man-
843 ual]. Retrieved from <https://CRAN.R-project.org/package=RColorBrewer>
844 (R package version 1.1-2)
- 845 Nie, W., Yuan, Y., Kepner, W., Nash, M. S., Jackson, M., & Erickson, C. (2011).
846 Assessing impacts of landuse and landcover changes on hydrology for the
847 upper san pedro watershed. *Journal of Hydrology*, 407(1), 105 - 114. Re-
848 trieved from [http://www.sciencedirect.com/science/article/pii/](http://www.sciencedirect.com/science/article/pii/S0022169411004549)
849 [S0022169411004549](http://www.sciencedirect.com/science/article/pii/S0022169411004549) doi: <https://doi.org/10.1016/j.jhydrol.2011.07.012>
- 850 OECD. (2016). *Financial management of flood risk*. Author. doi: 10.1787/
851 9789264257689-en
- 852 Ouazad, A., & Kahn, M. (2019, Sep). Mortgage finance in the face of rising climate
853 risk. *National Bureau of Economic Research Working Paper*. doi: 10.3386/
854 w26322
- 855 Paprotny, D., Sebastian, A., Morales-Nápoles, O., & Jonkman, S. N. (2018, May).
856 Trends in flood losses in europe over the past 150 years. *Nature Communica-*
857 *tions*, 9(1). Retrieved from [http://dx.doi.org/10.1038/s41467-018-04253-](http://dx.doi.org/10.1038/s41467-018-04253-1)
858 [-1](http://dx.doi.org/10.1038/s41467-018-04253-1) doi: 10.1038/s41467-018-04253-1
- 859 Pebesma, E. (2018). Simple Features for R: Standardized Support for Spatial Vec-
860 tor Data. *The R Journal*. Retrieved from [https://journal.r-project.org/](https://journal.r-project.org/archive/2018/RJ-2018-009/index.html)
861 [archive/2018/RJ-2018-009/index.html](https://journal.r-project.org/archive/2018/RJ-2018-009/index.html)
- 862 Pebesma, E. J., & Bivand, R. S. (2005, November). Classes and methods for spa-
863 tial data in R. *R News*, 5(2), 9–13. Retrieved from [https://CRAN.R-project](https://CRAN.R-project.org/doc/Rnews/)
864 [.org/doc/Rnews/](https://CRAN.R-project.org/doc/Rnews/)
- 865 Perrin, C., Michel, C., & Andréassian, V. (2013). A set of hydrological models. In
866 *Mathematical models* (p. 493-509). John Wiley & Sons, Ltd. Retrieved from
867 <https://onlinelibrary.wiley.com/doi/abs/10.1002/9781118557853.ch16>
868 doi: 10.1002/9781118557853.ch16
- 869 Powers, D. (2011). Evaluation: From precision, recall and f-measure to roc, in-
870 formedness, markedness and correlation. *Journal of Machine Learning Tech-*
871 *nologies*, 2(1), 37 - 63.
- 872 R Core Team. (2018). R: A language and environment for statistical computing
873 [Computer software manual]. Vienna, Austria. Retrieved from [https://www.R](https://www.R-project.org/)
874 [-project.org/](https://www.R-project.org/)
- 875 Rumsey, C. A., Miller, M. P., Susong, D. D., Tillman, F. D., & Anning, D. W.

- 876 (2015). Regional scale estimates of baseflow and factors influencing baseflow in
 877 the upper colorado river basin. *Journal of Hydrology: Regional Studies*, 4, 91 -
 878 107. Retrieved from [http://www.sciencedirect.com/science/article/pii/](http://www.sciencedirect.com/science/article/pii/S2214581815000373)
 879 [S2214581815000373](http://www.sciencedirect.com/science/article/pii/S2214581815000373) doi: <https://doi.org/10.1016/j.ejrh.2015.04.008>
- 880 Sampson, C. C., Smith, A. M., Bates, P. D., Neal, J. C., Alfieri, L., & Freer, J. E.
 881 (2015). A high-resolution global flood hazard model. *Water Resources Re-*
 882 *search*, 51(9), 7358-7381. Retrieved from <https://agupubs.onlinelibrary>
 883 [.wiley.com/doi/abs/10.1002/2015WR016954](https://agupubs.onlinelibrary.wiley.com/doi/abs/10.1002/2015WR016954) doi: 10.1002/2015WR016954
- 884 Shangguan, W., Dai, Y., Duan, Q., Liu, B., & Yuan, H. (2014). A global soil data
 885 set for earth system modeling. *Journal of Advances in Modeling Earth Sys-*
 886 *tems*, 6(1), 249-263. (Accessed data: 2018-8-6) doi: 10.1002/2013MS000293
- 887 Shangguan, W., Hengl, T., Mendes de Jesus, J., Yuan, H., & Dai, Y. (2017). Map-
 888 ping the global depth to bedrock for land surface modeling. *Journal of Ad-*
 889 *vances in Modeling Earth Systems*, 9(1), 65-88. (Accessed data: 2018-8-6) doi:
 890 10.1002/2016MS000686
- 891 Shi, W. (2007). Global daily surface air temperature analyses. *Presentation*.
 892 Retrieved from [ftp://ftp.cpc.ncep.noaa.gov/precip/PEOPLE/wd52ws/](ftp://ftp.cpc.ncep.noaa.gov/precip/PEOPLE/wd52ws/global_temp/CPC-GLOBAL-T.pdf)
 893 [global_temp/CPC-GLOBAL-T.pdf](ftp://ftp.cpc.ncep.noaa.gov/precip/PEOPLE/wd52ws/global_temp/CPC-GLOBAL-T.pdf) (Data Accessed: 2018-6-15)
- 894 Sing, T., Sander, O., Beerenwinkel, N., & Lengauer, T. (2005). Rocr: visualizing
 895 classifier performance in r. *Bioinformatics*, 21(20), 7881. Retrieved from
 896 <http://rocr.bioinf.mpi-sb.mpg.de>
- 897 Tapley, B. D., Bettadpur, S., Ries, J. C., Thompson, P. F., & Watkins, M. M.
 898 (2004). Grace measurements of mass variability in the earth system. *Science*,
 899 305(5683), 503-505. Retrieved from [https://science.sciencemag.org/](https://science.sciencemag.org/content/305/5683/503)
 900 [content/305/5683/503](https://science.sciencemag.org/content/305/5683/503) doi: 10.1126/science.1099192
- 901 Task Force on Climate-related Financial Disclosures. (2017). *Final report: Rec-*
 902 *ommendations of the task force on climate-related financial disclosures*. Task
 903 Force on Climate-related Financial Disclosures.
- 904 Vorogushyn, S., Bates, P. D., de Bruijn, K., Castellarin, A., Kreibich, H.,
 905 Priest, S., ... Merz, B. (2018). Evolutionary leap in large-scale flood
 906 risk assessment needed. *WIREs Water*, 5(2), e1266. Retrieved from
 907 <https://onlinelibrary.wiley.com/doi/abs/10.1002/wat2.1266> doi:
 908 10.1002/wat2.1266
- 909 Ward, P. J., Jongman, B., Kumm, M., Dettinger, M. D., Sperna Weiland, F. C., &
 910 Winsemius, H. C. (2014). Strong influence of el niño southern oscillation on
 911 flood risk around the world. *Proceedings of the National Academy of Sciences*,
 912 111(44), 15659-15664. doi: 10.1073/pnas.1409822111
- 913 Ward, P. J., Jongman, B., Salamon, P., Simpson, A., Bates, P., De Groeve, T.,
 914 ... Winsemius, H. C. (2015, Jul). Usefulness and limitations of global
 915 flood risk models. *Nature Climate Change*, 5(8), 712-715. Retrieved from
 916 <http://dx.doi.org/10.1038/nclimate2742> doi: 10.1038/nclimate2742
- 917 Ward, P. J., Winsemius, H. C., Kuzma, S., Bierkens, M. F., Bouwman, A., De Moel,
 918 H., ... Luo, T. (2020). Aqueduct floods methodology. *Technical Note*. Re-
 919 trieved from www.wri.org/publication/aqueduct-floods-methodology
- 920 Winsemius, H. C., Van Beek, L. P. H., Jongman, B., Ward, P. J., & Bouw-
 921 man, A. (2013). A framework for global river flood risk assessments.
 922 *Hydrology and Earth System Sciences*, 17(5), 1871-1892. Retrieved
 923 from <https://www.hydrol-earth-syst-sci.net/17/1871/2013/> doi:
 924 10.5194/hess-17-1871-2013
- 925 Wolock, D. M., Winter, T. C., & McMahon, G. (2004, Apr). Delineation and eval-
 926 uation of hydrologic-landscape regions in the united states using geographic
 927 information system tools and multivariate statistical analyses. *Environmental*
 928 *Management*, 34(S1), S71-S88. Retrieved from [http://dx.doi.org/10.1007/](http://dx.doi.org/10.1007/s00267-003-5077-9)
 929 [s00267-003-5077-9](http://dx.doi.org/10.1007/s00267-003-5077-9) doi: 10.1007/s00267-003-5077-9
- 930 Xie, P., Chen, M., Yang, S., Yatagai, A., Hayasaka, T., Fukushima, Y., & Liu, C.

- 931 (2007). A gauge-based analysis of daily precipitation over east asia. *Jour-*
932 *nal of Hydrometeorology*, 8(3), 607-626. (Data Accessed: 2018-6-18) doi:
933 10.1175/JHM583.1
- 934 Yamazaki, D., Kanae, S., Kim, H., & Oki, T. (2011). A physically based descrip-
935 tion of floodplain inundation dynamics in a global river routing model. *Water*
936 *Resources Research*, 47(4). Retrieved from [https://agupubs.onlinelibrary](https://agupubs.onlinelibrary.wiley.com/doi/abs/10.1029/2010WR009726)
937 [.wiley.com/doi/abs/10.1029/2010WR009726](https://agupubs.onlinelibrary.wiley.com/doi/abs/10.1029/2010WR009726) doi: 10.1029/2010WR009726
- 938 Yu, Z., Gburek, W. J., & Schwartz, F. W. (2000). Evaluating the spatial distribu-
939 tion of water balance in a small watershed, pennsylvania. *Hydrological Pro-*
940 *cesses*, 14(5), 941-956. Retrieved from [https://onlinelibrary.wiley.com/](https://onlinelibrary.wiley.com/doi/abs/10.1002/%28SICI%291099-1085%2820000415%2914%3A5%3C941%3A%3AAID-HYP2%3E3.0.CO%3B2-S)
941 [doi/abs/10.1002/%28SICI%291099-1085%2820000415%2914%3A5%3C941%3A%](https://onlinelibrary.wiley.com/doi/abs/10.1002/%28SICI%291099-1085%2820000415%2914%3A5%3C941%3A%3AAID-HYP2%3E3.0.CO%3B2-S)
942 [3AAID-HYP2%3E3.0.CO%3B2-S](https://onlinelibrary.wiley.com/doi/abs/10.1002/%28SICI%291099-1085%2820000415%2914%3A5%3C941%3A%3AAID-HYP2%3E3.0.CO%3B2-S) doi: 10.1002/(SICI)1099-1085(20000415)14:
943 5<941::AID-HYP2>3.0.CO;2-S

Database	Variable	Data Reference
Response variables		
DFO - Dartmouth Flood Observatory Global Active Archive of Large Flood Events	Flood event Population displaced	Brakenridge (2010)
Predictor variables		
CHIRPS - Climate Hazards group Infrared Precipitation with Stations	Precipitation (Daily, 1981-present) (0.05°) For sites between $[-50^\circ, +50^\circ]$ latitude	Funk (2015)
CPC Precipitation - CPC Global Unified Gauge-Based Analysis of Daily Precipitation	Precipitation (Daily, 1979-present) (0.5°) For sites outside $[-50^\circ, +50^\circ]$ latitude	Xie et al. (2007)
CPC Temperature - CPC Global Daily Temperature	Temperature (Daily, 1979-present) (0.5°)	Shi (2007)
HydroBASINS	Aspect Elevation Hillslope Slope Topographic position index Latitude of watershed centroid Longitude of watershed centroid	Lehner and Grill (2013)
TI - High-resolution global topographic index values	Topographic index	Marthews et al. (2015a)
GLC-SHARE - Global Land Cover SHARE	Artificial surfaces Cropland Grassland Tree covered areas Shrubs covered areas Herbaceous vegetation Aquatic or regularly flooded Mangroves Sparse vegetation Bare soil Snow and glaciers Water bodies	Latham et al. (2014)
GSD - Global Soil Dataset for Earth System Modeling	Sand Silt Clay Gravel Bulk soil density	Shangguan et al. (2014)
GDB - Global depth to bedrock	Global depth to bedrock	Shangguan et al. (2017)
GLHYMPS 2.0 - GLobal HYdrogeology MaPS 2.0	Bedrock porosity Bedrock permeability	Gleeson et al. (2014)
GPW - Gridded Population of the World	Population count (2.5 min)	CIESIN (2018)
HYDE3.2 - Anthropogenic land-use estimates for the Holocene	Population count (5 min)	Klein Goldewijk (2017)
GDPHDI - Gridded global datasets for GDP and HDI over 1990-2015	Gross domestic product (PPP) per capita (5 min)	Kummu et al. (2019)

Table 1. Response and predictor variables used in statistical fits of occurrence and impact models.

Variable Long Name	Variable	Model Quantity
Atmospheric rain	RAIN	Precipitation
Atmospheric snow	SNOW	Precipitation
Reference height temperature	TREFHT	Temperature

Table 2. Forcing climate variables from the NCAR CESM Large Ensemble (CESM-LE) Community Project.

Step	Description	Duration	Repetitions
1	Occurrence - Simulation	1.34 s / simulation	625
2	Intensity - Distribution mean	36.9 min / member	40
3	Intensity - Distribution standard deviation	3.1 s	1
4	Intensity - Merge mean and standard deviation	6.8 s	1
5	Simulate intensity and combine with occurrence	3.75 s / simulation	50
6	Calculate standard deviation correction	1.68 min	1
7	Repeat step 4 with corrected standard deviation	6.8 s	1
8	Simulate corrected intensity and combine with occurrence	3.75 s / simulation	625

Table 3. Duration of simulation computation steps.

Model	Global Fit	HS2 Fit
LR	0.735	0.789
RF	0.788	0.792
NN-24	0.787	-
NN-12-12	0.781	-
NN-24-24	0.776	-
NN-12	-	0.777

Table 4. Out-of-sample area under the ROC curve for occurrence models and fitting approaches considered.

	Mean decrease in accuracy	Mean decrease in Gini impurity index
1	GDP per capita	Population density
2	Population density	Precipitation (previous 7 days)
3	Temperature (annual mean)	GDP per capita
4	Precipitation (previous 7 days)	Precipitation (previous 8-30 days)
5	Topographic position index	Precipitation (previous 31-60 days)
6	Precipitation (previous 8-30 days)	Precipitation (previous 61-120 days)
7	Gravel	Temperature (annual mean)
8	Precipitation (previous 61-120 days)	Cropland
9	Aspect	Latitude
10	Porosity	Longitude

Table 5. Most significant predictors of flood occurrence ranked by two methods for the globally fitted random forest model.

Model	Global Fit	HS2 Fit
LM	0.172	0.209
RF	0.325	0.353
NN-26	0.291	-
NN-13-13	0.287	-
NN-26-26	0.303	-
NN-13	-	0.308

Table 6. Out-of-sample R^2 for impact models and fitting approaches considered.

	Increase in mean squared error	Increase in residual sum of squares
1	Precipitation (previous 8-30 days)	GDP per capita
2	GDP per capita	Temperature (previous 61-120 days)
3	Precipitation (previous 7 days)	Temperature (previous 31-60 days)
4	Population density	Temperature (previous 8-30 days)
5	Precipitation (previous 31-60 days)	Temperature (previous 7 days)
6	Precipitation (previous 61-120 days)	Population density
7	Temperature (previous 61-120 days)	Precipitation (previous 7 days)
8	Temperature (previous 7 days)	Latitude
9	Longitude	Precipitation (previous 31-60 days)
10	Temperature (previous 31-60 days)	Precipitation (previous 8-30 days)

Table 7. Most significant predictors of impact model ranked by two methods.